Determination of surface concentrations of individual molecule-layers used in nanoscale biosensors by in-situ ATR-FTIR spectroscopy

Manuel Punzet[a], Dieter Baurecht*[a], Franz Varga[b], Heidrun Karlic[c], and Clemens Heitzinger[d,e]

[a]Institute of Biophysical Chemistry, University of Vienna, Althanstraße 14, A-1090 Vienna, Austria. E-mail: dieter.baurecht@univie.ac.at
[b]Ludwig Boltzmann Institute of Osteology, Hanusch Hospital, Heinrich Collin-Straße 30, A-1140 Vienna, Austria
[c]Ludwig Boltzmann Institute for Leukemia Research and Cluster Oncology, Hanusch Hospital, Heinrich Collin-Straße 30, A-1140 Vienna, Austria
[d]Department of Mathematics, University of Vienna, Nordbergstrasse 15, A-1090 Vienna, Austria
[e]Department of Applied Mathematics and Theoretical Physics (DAMTP), University of Cambridge, Cambridge CB3 0WA, UK

Abstract

For the development of nanowire sensors for chemical and medical detection purposes, the optimal functionalization of the surface is a mandatory component. Quantitative ATR-FTIR spectroscopy was used in-situ to investigate the step-by-step layer formation of typical functionalization protocols and to determine the respective molecule surface concentrations. BSA, anti-TNF-α and anti-PSA antibodies were bound via 3-(trimethoxy)butylsilyl aldehyde linkers to silicon-oxide surfaces in order to investigate surface functionalization of nanowires. Maximum determined surface concentrations were 7.17 e-13 mol/cm^2 for BSA, 1.7 e-13 mol/cm^2 for anti-TNF-α antibody, 6.1 e-13 mol/cm^2 for anti-PSA antibody, 3.88 e-13 mol/cm^2 for TNF-α and 7.0 e-13 mol/cm^2 for PSA. Furthermore we performed antibody-antigen binding experiments and determined the specific binding ratios. The maximum possible ratios of 2 were obtained at bulk concentrations of the antigen in the µg/ml range for TNF-α and PSA.

Keywords

nanowire biosensor, nanosensor, field-effect sensor, FTIR, ATR, antibody, antigen, PSA, TNF-α, BSA, surface concentration, chemical functionalization, quantitative spectroscopy.

Introduction

The development of nanoscale sensor devices for the label-free detection [1-4] of DNA and various biological markers plays an important role in future medical diagnostic systems. Current devices work via piezoelectric effects [5, 6], in combination with field effects [7], via nanomechanical effects [8-11] or as semi-conductor field-effect transistors (FET) [2, 12, 13]. Fields of application involve structural monitoring and sensing of biological molecules and chemical compounds such as the detection of cancer markers in blood analysis [2, 14]. In the case of field-effect nanowire sensors, the binding of target molecules changes the charge concentration at the surface; this effect acts like a gate contact and modulates the current through the transducer. Advantages of this technique are the direct conversion of a chemical or biochemical signal to an electrical signal without any intermediates like fluorescent markers or optical systems, i.e. a label-free detection is achieved. The sensitivity of nanowire sensors is unparalleled with detection limits for DNA in the femtomolar range [12, 15], and proteins can be detected in the picomolar range [16].

Although methods for surface functionalization are known [14, 17, 18], the density of the functionalized layer depends on many process parameters of the single steps of surface functionalization including the attachment of linkers. Without the ability to check the quality of the single steps of surface functionalization, it is very time consuming to determine the influence of the various process parameters. Therefore in-situ FTIR measurements were used in this work to characterize the step-by-step formation of the functionalized surface.

FTIR spectroscopy is well-known to be able to characterize chemical modifications of surfaces by the use of attenuated total reflection (ATR) [19-32], infrared reflection-absorption spectroscopy (IRRAS) [33] or grazing-angle attenuated total reflection (GATR) [18]. The former is also able to quantitatively determine surface concentrations [34, 35]. As FTIR-ATR techniques directly measure chemical information of the molecules, we can quantify molecule concentrations on the chemical basis of functional groups of the unmodified molecules. This is a considerable advantage compared to techniques that need molecular

labeling (e.g. fluorescence measurements), techniques that are only able to measure the changes of masses (e.g. quartz crystal microbalance measurements) or techniques that use relatively unspecific changes of the refractive indices without the information from which molecules these changes results from (e.g. surface plasmon resonance measurements).

In this work, we determined surface concentrations of proteins attached to silicon-oxide surfaces by FTIR-ATR spectroscopy. Moreover, we determined resulting antibody-antigen ratios for two different systems. The fact that silicon is not only used as the semiconducting transducer, but also serves as an internal-reflection element in FTIR-ATR-spectroscopy, offers the ability to investigate silicon-oxide surfaces by FTIR-spectroscopy. We also demonstrate how to use FTIR-ATR spectroscopy as a tool for the determination of surface concentrations of monomolecular layers and chemical binding properties of surface modifications utilized in nanowire sensors. This method can be used to optimize surface-modification protocols, which are essential for the development of nanowire sensors.

The resulting data is also used in numerical simulations in order to provide the quantitative understanding of the sensing mechanism of field-effect sensors. To this end, a self-consistent partial-differential-equations model [36-38] was developed as well as a Metropolis-Monte-Carlo algorithm [39] for the quantification of screening by free ions. Other screening models have been developed as well [40, 41]. Using our simulations, we can determine optimal device parameters and the optimal operating regime [42-44].

Experimental

Chemicals

Bovine serum albumin (BSA) was bought from Sigma-Aldrich. 3-(trimethoxy)butylsilyl aldehyde was purchased from United Chemical Technologies, Inc. (Bristol). Prostate-specific antigen antibody was purchased from Fisher Scientific and Prostate specific antigen (PSA) from Calbiochem. Human tumor necrosis factor-alpha (TNF-α) was purchased from Stratham Biotec AG. Monoclonal hTNF-α antibody was obtained from the Center for Biomedical Technology, Danube University, Krems (Austria). PTFE syringe filters with 20 μm cut-off were purchased from Sartorius (Germany). 10 mM potassium and sodium phosphate buffer at pH 8.4 were used as buffer during the binding of all proteins to the silane surface. For the antigen capture experiments 10 mM potassium phosphate and 10 mM sodium phosphate at pH 7.4 with additional 2 μM KCl were used as buffer solution. 96% ethanol was prepared with spectroscopic grade absolute ethanol and ultra pure water. All aqueous solutions were prepared using ultra pure water and degassed prior to use.

FTIR measurements

All FTIR-ATR spectra were measured at 25°C with a Bruker IFS 66 FTIR spectrometer using a MCT detector. Trapezoidal shaped multiple internal reflection elements (MIRE, base length 52 mm, width 20 mm thickness 1.5 mm) made of silicon were used as ATR-elements. The surface was chemically polished with a polishing machine (Logitech PM-5) using amorphous silica suspension (Logitech SF-1) on a polyurethane polishing cloth (Logitech). After polishing and cleaning, the element was refluxed for 4 h in 70% nitric acid to activate the silicon surface by oxidation and remove any metal ions interfering with the silanization reaction later. The final preparation step was a 3 min plasma cleaning (Harrick Plasma cleaner). For polarization of the incident IR-beam an aluminum grid polarizer on a KRS-5 substrate (Specac, Orpington, U.K.) was used. The ATR angle of incidence Θ was set at 45°. FTIR spectra were recorded at 4 cm^{-1} resolution using Blackham-Harris 3-term apodization and a zero filling factor of 4. Interferograms were measured in double sided mode that needs no phase correction, due to small sample absorbancies in a high background absorbance, e.g. H_2O of buffer. Thermostated flow-through cells made of Delrin® were used to mount the MIREs and to simultaneously surround the measurement compartments. To determine molar absorbance coefficients, transmission spectra were recorded using a Bruker IFS 25 with a DTGS detector at 4 cm^{-1} resolution using single-sided mode and Mertz phase correction. The transmission cell consisted of calcium fluoride windows and Mylar® spacers with a determined real thickness of 24.7 μm [45]. Spectrometers were constantly purged with dry, carbon dioxide free air and set up on optical tables. Peristaltic pumps are used to fill or rinse the compartments of the flow-through cell holding the MIRE. To

achieve a relevant signal-to-noise ratio 3000 to 4000 scans were necessary in the protein experiments to properly evaluate the surface concentrations. For determining the surface concentration of the silane layers 500 to 1000 scans were sufficient.

SBSR-measuring technique

As the quantitative IR-spectroscopic detection of molecular monolayers requires extremely accurate and sensitive methods, the single-beam sample-reference (SBSR) measurement method [35] was used to compensate absorbancies from bulk water in sample and reference. Fluctuations of the absorbance of remaining water vapor and carbon dioxide during the measurement of sample and reference are also reduced to a minimum by this method. The flow-through cell separates the MIRE horizontally in a sample and a reference compartment. It is attached on a stage and can be vertically moved in the IR-beam by a computer controlled lift to alternately measure spectra of the sample and reference compartments and allows an outstanding compensation of water absorbance. This is crucial, since proteins are typically quantified according to their amide I (1640 cm^{-1}) and amide II (1540 cm^{-1}) vibrations any additional uncompensated water absorbance between sample and reference deteriorates the results. Differences in the transmission properties of the MIRE in the sample and reference compartments were recorded before surface modifications and considered when calculating the final difference spectra of the samples.

Calculation of the surface concentration

The surface concentration Γ may be understood as the projection of the molecules in the volume defined by unit area and height d (real sample thickness). As a consequence, surface concentration of a thin layer can be determined without knowing the real thickness d and its real structure. The calculation is based on Lambert-Beer's law. For the ATR technique the introduction of the so-called "effective thickness" d_e first introduced by Harrick is required [20, 35, 46]. The volume concentration c and the surface concentration Γ are related to each other via the thickness d of the sample. By introducing Lambert-Beer's law one obtains

$$c = \frac{\Gamma}{d} = \frac{\int A_{pp|vp}(\tilde{v})d\tilde{v}}{N\,n\,d_{e,pp|vp}^{th}\,\int \varepsilon(\tilde{v})d\tilde{v}} \tag{1}$$

$\int A_{pp|vp}(\tilde{v})d\tilde{v}$ denotes the integrated absorbance of a distinct absorbance band measured with parallel (pp), or perpendicular (vp) polarized incident light, respectively. N is the mean number of the active internal reflections and n denotes the number of equal infra-red active groups per molecule leading to the absorbance of the evaluated bands. $\int \varepsilon(\tilde{v})d\tilde{v}$ denotes the common integrated molar absorption coefficient of the vibrational mode of one infra-red active group. $d_{e,pp|vp}^{th}$ is the effective thickness of the layer which depends on the polarization, the angle of incidence and the refractive indices of the MIRE and the sample. $d_{e,pp|vp}^{th}$ is regarding the theory of ATR the crucial value to be determined. In case of anisotropic samples (1) would lead to different results for parallel and vertical polarized light. Therefore the absorbance of both polarization directions has to be determined and to be considered in the calculation of the surface concentration using a model for the orientation of the molecules [35]. Here we used the model of liquid crystalline ultrastructure (LCU) for the calculation of surface concentrations. This model best fits the distribution of orientation of silanes and is also correct for isotropic distributions of molecules. For proteins the isotropic distribution was ensured by the determination of the dichroic ratio $R_{exp.}$ (2) that has to be equal to the theoretical dichroic ratio R_{iso}^{th} = 1.63 valid for thin layers and the used optical parameters of ATR measurements.

$$R_{exp.} = \frac{\int A_{pp}(\tilde{v})d\tilde{v}}{\int A_{vp}(\tilde{v})d\tilde{v}} \tag{2}$$

As in the experiments with TNF-α the signal-to-noise ratio of the vp-measurements was very poor, the surface concentrations of TNF-α and its antibody where directly determined by the evaluation of (1) using results from pp measurements. The reader is referred to [20, 34, 35, 46] for more details of the quantitative

evaluation of molecular surface densities using ATR technique. Optical parameters used in the calculations are $45° \pm 5°$ angle of incidence, and refractive indices at wavenumber 1540 cm^{-1} for silicon (3.42 ± 0), water (1.33 ± 0.06) and sample layer (1.45 ± 0.06). The number of active internal reflections was different in different experiments and is given in figure 2. Quantifications for all proteins were done by determining the absorbance of the amide II band that is only barely effected by uncompensated water absorbance. Nevertheless, the integrated absorbance was evaluated after compensation of the small negative water band at 1640 cm^{-1} by adding an appropriate amount of a pure water spectrum. We emphasize that this small amount of uncompensated water results from water present in the reference compartment but replaced by the molecules of the bound layer in the sample compartment and therefore it can never be experimentally removed. The amount of added water absorbance was estimated by the remaining absorbance of the H$_2$O stretching vibration and by evaluating the ratio between integrated absorbancies of amide I and amide II vibrations. The resulting ratios were between 1.45 and 2.68 with a mean value of 2.25 for parallel polarized light and between 2.21 and 3.81 with a mean value of 2.63 for vertical polarized light. Estimated values of the error of integrated absorbancies are between 5 % and 30 % depending on the signal-to-noise levels of spectra and remaining uncompensated water absorption. All errors in the calculation of surface concentrations and dichroic ratios are evaluated using propagation of uncertainty.

Determination of molar absorption coefficients

FTIR transmission-spectra of 3-trimethoxysilylbutyl aldehyde dissolved in different concentrations in 96% EtOH where measured and integrated absorbancies of the C=O vibration were determined using integration limits of 1751 ± 1 and 1693 ± 1 cm^{-1}. The resulting average integral molar absorption coefficient of the C=O vibration of 3-trimethoxysilylbutyl aldehyde was 8.6 e5 ($\pm$ 2.9 e5) cm/mol. Ethanolamine was dissolved in 10 mM phosphate buffer and the integrated absorbance of the CH$_2$ symmetric stretch vibration determined. The integration limits were set at 2867 ± 1 and 2831 ± 1 cm^{-1}. The resulting molar absorption coefficient was 1.18 e6 cm/mol. The value for the molar absorption coefficient of one amide bond of the amide II vibrational mode of BSA was determined by Reiter et al. [19] as 8.25 e6 cm/mol with integration limits at 1585 ± 1 and 1500 ± 1 cm^{-1} (for proteins, the molar absorption coefficient is related to single amide bondings and not to the whole molecules).

Silanization of silicon MIREs using 3-(trimethoxy)butylsilyl aldehyde

According to the protocol of Patolsky et al. [14] a solution of 1% 3-(trimethoxy)butylsilyl aldehyde in 96% EtOH was filtered with a 20 μm cut-off PTFE syringe filter after a 20 min waiting period and pumped into the sample compartment of the flow-through cell. The reaction time to form hydrogen bonds with the silanol groups (Fig.1) of the silicon-oxide surface was 30 min. Afterwards, the sample-compartment was carefully rinsed with 96% ethanol (2 μl/s) to flush out any unbound silane. After drying with nitrogen gas, the system was exposed to a temperature of 80°C for 30 min to form covalent bonds between silane and the silicon-oxide surface. Precursor experiments showed that these parameters lead to a high surface concentration of covalently bound silane. As last step, the silane layer on silicon is thoroughly rinsed with 96% EtOH to remove any non-covalently bound silane from the surface with a flow rate of 15 μl/s. The silane surface concentration of every silanization was quantified to ensure consistent and uniform conditions for subsequent protein attachment.

Protein binding to aldehyde surface

The proteins are either reconstituted or diluted in 10 mM sodium or potassium phosphate buffer with a pH of 8.4 additionally containing 4 mM sodium cyanoborohydrid (NaCNBH$_3$). The protein solution was pumped over the silanized surface through the sample-compartment of the flow-through cell with a very low flow-rate of 42 μl/min avoiding any depletion effects. Free amino groups of the proteins can then form imines (Schiff's bases) with the aldehyde moieties of the silane layer. Subsequently imines are reduced by cyanoborohydride to amide bonds leading to covalent bonding of proteins and silane. After a 2 h reaction period, superfluous protein was washed out by rinsing with buffer solution.

Passivation of aldehyde surface

Since not every aldehyde moiety of the silane-layer binds proteins, the remaining CHO-groups must be capped to prevent any unspecific binding in further antibody experiments. This was done by filling the sample-compartment for 2 h with 100 mM ethanolamine containing 4 mM cyanoborohydride in a phosphate buffer at a pH of 8.4.

Antigen capturing with antibody layer

Antigen solutions of TNF-α and PSA in phosphate buffer with a pH of 7.4 were pumped onto the respective antibody layers and left for 2 h to ensure thorough antigen-antibody contact. Afterwards superfluous antigen that was not bound to the antibodies was washed out with phosphate buffer.

Results and discussion

Surface concentration of 3-(trimethoxy)butylsilyl aldehyde

3-(trimethoxy)butylsilyl aldehyde was covalently bound to the silicon-oxide surface serving as basic linker molecule for all further chemical modification steps. The measured surface concentrations evaluated from the absorbance of the C=O vibration (Fig.2A) were between 6.0 e-10 mol/cm^2 and 1.2 e-9 mol/cm^2 with optimized protocols for silanization. A theoretical value of the surface concentration of a densely packed monolayer can be estimated by simple two-dimensional geometrical calculations of the molecule [47] and results in 4.88 e-10 mol/cm^2, which perfectly matches our measured values. Differences in surface concentrations can be caused by the nanoscale surface roughness of the MIRE resulting in an increased surface area and by the polymerization processes of trimethoxy silanes that can lead to different chain lengths and therefore a multilayer arrangement [48]. Indeed, already small changes in the preparation protocols such as the curing temperature and time, treatment of the semiconductor surface or the dwell-time of silane before the start of polymerization led to highly differing surface concentrations up to 2.0 e8 mol/cm^2 in preliminary experiments. Only by the use of the quantitative evaluation of this step, we were able to establish a preparation protocol leading to reproducible and meaningful results.

Bovine serum albumin (BSA) on aldehyde silane layer

Since BSA is one of the most used and best characterized proteins, a measurement system was developed to determine the surface concentration and the workability of the linker protocol. BSA is known to exhibit considerable adhesion and to form densely packed layers on a variety of surfaces including germanium MIREs in IR-spectroscopy [49-51], mica platelets [52] and gold stripes [53] used in atomic force microscopy. The number of functional amide bonds is 582. Following experiments were conducted to determine the maximum possible surface concentration of BSA covalently bound on an aldehyde-silanised silicon-oxide surface. We utilized a solution of BSA with a concentration of 100 µg/ml prepared in 10 mM phosphate buffer at a pH of 7.4 and pumped it into the flow-through cell containing the silanised surface of a silicon MIRE. The protein solution was allowed to adsorb for 2 h followed by a buffer rinse to remove the bulk protein solution. Adsorption of BSA was investigated by evaluating the absorbance of the amide II vibration (Fig.2B). Resulting BSA surface concentrations were in the range of 5.62 – 7.17 e-13 mol/cm^2. This means one molecule of BSA is found at a space of 295 nm^2 to 232 nm^2. Compared to the maximum achieveable surface concentration of 5.7 e-12 mol/cm^2 documented by Hassler et al. [54] the values are lower by an order of magnitude. However the experimental conditions were significantly different. Hassler used a germanium MIRE, a 25 mg/ml protein concentration and high concentrations of sodium chloride, which shields the charges of the proteins [39, 55] and the germanium surface ultimately forming a BSA monolayer. Albumins mainly act as transport molecules in a living body and are known to be capable of binding chloride ions [56]. Luey et al.[57] showed that an increase in ionic strength leads to higher surface concentrations on silicon due to the shielding effect negatively charged ions have on the protein itself. Although in our experimental setup the surface charges of the silanol-groups are blocked by the aldehyde

silane, electrostatic repulsion between the individual BSA molecules is still taking place possibly leading to a reduced surface concentration.

Surface concentrations of anti-TNF-α antibody on silanised silicon and captured TNF-α

The antibody/antigen system anti-TNF-α antibody and TNF-α was investigated using the bound antibody as receptor molecules to specifically bind its antigen that should be detected in case of a biosensor. The number of functional amide bonds of all IgG antibodies is 1320 (± 4) and the number of functional amide bonds of TNF-α is 468. A protein solution of 100 μg/ml of anti-TNF-α antibody in 10 mM sodium phosphate buffer at pH 8.4 was pumped onto an aldehyde silane layer with additional 4 mM cyanoborohydride. After 2 hours, the bulk protein solution including only adhered antibody was flushed out with buffer solution at pH 7.4. Quantification of the amide II vibrations in this state resulted in surface concentrations between 1.6 e-13 mol/cm^2 and 1.7 e-13 mol/cm^2 for the anti-TNF-α antibody. This corresponds to a used area of 1000 nm^2 per molecule or a side length of 31 nm assuming square cross sections. The diameter of IgG antibodies differs in literature between 16 nm [58] and 28 nm [59], corresponding to required areas per molecule of 256 nm^2 to 784 nm^2 assuming square cross sections. Therefore, in case of anti-TNF-α antibody an almost closed monolayer bound to the silanised surface can be supposed. After providing TNF-α bulk concentrations between 1 μg/ml and 18 μg/ml to the bound anti-TNF-α antibody molecules, the surface concentration of antibody-bound TNF-α resulted in 1.7 e-13 mol/cm^2 to 2.7 e-13 mol/cm^2 corresponding to an antigen/antibody ratio between 1.0 and 1.6 (Fig.3). Since one IgG antibody molecule can at best bind two antigens, this shows that almost all possible binding sites of the antibody specifically bound antigens. Below a bulk concentration of 1 μg/ml, TNF-α could neither be detected in the bulk solution nor captured on the surface. The smallest detectable absorption amplitude in the amide II region was 50 μAU. This means the detection limit for TNF-α was 2.6 e-14 mol/cm^2.

Anti-PSA-antibody and PSA on aldehyde surface

As a second antibody/antigen system PSA-antibody and PSA was investigated. This system was already used in a prototype nanosensor by Patolsky et al. [14]. Here the number of amide bonds of PSA is 237. A solution of mouse anti-PSA antibody with a concentration of 50 μg/ml in 10 mM potassium phosphate buffer at a pH of 8.4 and additional 4 mM cyanoborohydride was pumped onto the aldehyde-surface and left for 2 h (Fig.2C). Surface concentrations of PSA-antibody were determined in the range of 3.2 – 6.1 e-13 mol/cm^2. The area used by each antibody molecule results in 270 nm^2 to 520 nm^2. Again, this agrees very well with the required area per molecule for an IgG antibody. After passivation with ethanolamine various PSA-antigen concentrations in the range of 5 ng/ml to 10 μg/ml in 10 mM potassiumphosphate buffer, pH 7.4 with additional 2 μM KCl were slowly pumped (42 μl/min) over the antibody surface for 2 h. (Fig.2D) The calculated antigen surface concentrations could be determined to be between 1.6 e-13 mol/cm^2 to 7.0 e-13 mol/cm^2. The resulting ratio of antigen to antibody could be determined between 0.3 to 1.4, again showing a suitable value for specific binding of the antigen. At PSA-antigen solutions with concentrations between 5 ng/ml and 500 ng/ml no evaluable amide vibration bands of the antigen could be detected neither in the spectra of the bulk solution nor in the spectra of the layer after washing. The smallest detectable amplitude for PSA was 100 μAU resulting in a surface concentration of 5.13 e-14 mol/cm^2. To determine the concentration of ethanolamine used for surface passivation after protein binding, we evaluated the increase of absorbance of the symmetric CH$_2$ vibration resulting from the passivation step (Fig.2E). The ethanolamine surface concentration was 2.30 e-10 mol/ cm^2 in PSA experiments. This means that about one third of the aldehyde moieties of the silane layer are capped with ethanolamine after PSA was bound to the silane.

Conclusions

Regarding the use of semiconductors as transducers, we point out that the resulting surface concentration of bound molecules on such surfaces is very sensitive to a variety of parameters of the surface chemistry used. With the ability of quantitative analysis of each layer, one can detect unexpected results in an early stage of the surface modification. We showed that it is possible to cover the whole silanised surface with an almost

compact monolayer only showing a slightly different surface concentration for different proteins (Table 1). As the proteins used are of the same size, the differences likely result from the different partial charges of the proteins. Thus it is possible to cover semiconductor nanostructures with a compact monolayer of receptor molecules for sensing purposes. Again, we want to emphasize that the optimum result of a compact monolayer is easily disrupted by non-optimal steps in the surface modification. It is a time consuming procedure to find the reasons for varying results without the ability to quantitatively assess each step during surface functionalization.

Antigen-Antibody binding can be well detected and quantified by the present method when the bulk concentrations of the antigen is above 1 µg/ml. This shows that almost all possible binding sites of the antibody are able to bind antigens. Therefore achievable surface concentrations of target molecules are only limited by the size of the receptor molecules and their binding sites, unless the molecules are highly charged.

Acknowledgements

Table 1: Surface concentrations of single molecule layers.

molecule	concentration of bulk solution	measured surface concentration [mol/cm^2]	error of surface concentration [mol/cm^2]	corresponding area per molecule [nm^2]	required area per molecule in literature [nm^2]
3-(trimethoxy) butylsilyl aldehyde	10 mg/ml	7.0 e-10	1.10 e-10	0.23	0.34
BSA	100 µg/ml	5.62 e-13 - 7.17 e-13	9.79 e-14 - 1.17 e-13	295 - 232	56 [19]
anti-TNF-α	100 µg/ml	1.6 e-13 - 1.7 e-13	4.68 e-14	1100 - 970	784 [59], 256 – 361[58]
anti-PSA	50 µg/ml	3.2 e-13 - 6.1 e-13	3.0 e-14 – 6.0 e-14	520 - 270	784 [59], 256 – 361[58]
TNF-α	1 – 18 µg/ml	8.61 e-14 - 3.88 e-13	2.2 e-14 - 4.12 e-14	ratio: TNF-α/anti-TNF-α, 0.5 - 2.2	
PSA	0.5 – 10 µg/ml	7.7 e-14 - 7 e-13	1.68 e-14 – 7.9 e-14	ratio: PSA/anti-PSA, 0.2 – 3 (5.1)	

Figure Legends

Fig. 1: Chemical scheme of surface functionalization of a silicon MIRE with 3-(trimethoxy)butylsilyl aldehyde and covalent bonding of proteins.

Fig. 2: FTIR-ATR absorbance spectra of single components for the setup of an antibody/antigen biosensor. Spectra were measured in situ during the layer by layer formation. (A) FTIR-ATR absorbance spectrum of 3-(trimethoxy)butylsilyl aldehyde in 96% ethanol. The quantitatively evaluated band is the C=O (carbonyl) vibration of the tail-group of the used silane (see Fig.1 for structure) at 1720 cm^{-1}. It indicates free carbonyl groups of silane on the silicon-oxide surface ready to form imine bonds. Other bands are caused by EtOH and H_2O incompensations despite the SBSR measurement method. Reference was blank silicon. Spectrum recorded with 1000 scans. (B) FTIR-ATR absorbance spectrum of BSA on aldehyde silane surface. The amide I (1640 cm^{-1}) and amide II (1540 cm^{-1}) bands are clearly distinguishable. Only the amide II band is used for the quantitative evaluation of the surface concentration, because amide I can be overlapped by uncompensated absorption of the water bending vibration. Other prominent bands are incompensations of the H_2O stretching vibration at 3400 cm^{-1} and the gaseous CO_2 stretching vibration at 2400 cm^{-1}. Reference was silanised silicon. Spectrum recorded with 3000 scans. (C) FTIR-ATR absorbance spectrum of anti-PSA antibody on aldehyde silane surface. Reference was silanised silicon. Recorded with 3000 scans. (D) FTIR-ATR absorbance spectrum of prostate specific antigen (PSA) on antibody surface. Reference was the ethanolamine passivated antibody layer on silanised silicon. Spectrum recorded with 3000 scans. (E) FTIR-ATR absorbance spectrum of ethanolamine on antibody surface. The symmetric CH_2 vibration was quantified. Reference was the antibody layer on silanised silicon. Spectrum recorded with 3000 scans. Spectroscopic parameters for all experiments were silicon MIRE, 45° angle of incidence and 10 mM phosphate buffer. Number of active internal reflections: 26(±1) for TNF-α, 28(±1) for PSA experiments.

Fig. 3: (A) TNF-α surface concentrations resulting from specific binding to anti-TNF-α antibody with a surface concentration of 1,76 e-13 Mol/cm^2. (B) The ratio of antigen to antibody exhibits the expected exponential shape asymptotically approaching the value of two, which is the maximum possible binding capability of an IgG antibody.

Fig. 4: (A) PSA surface concentrations on anti-PSA antibody surface in five different experiments. Antibody concentration of each experiment is shown at bulk concentration zero. (B) Ratio of antigen to antibody in several experiments. Since two antigens is the maximum possible binding capability of an IgG antibody values exceeding two point to unspecific adhesion to the surface. This occurred only in one experiment at very high bulk concentrations of the antibody.
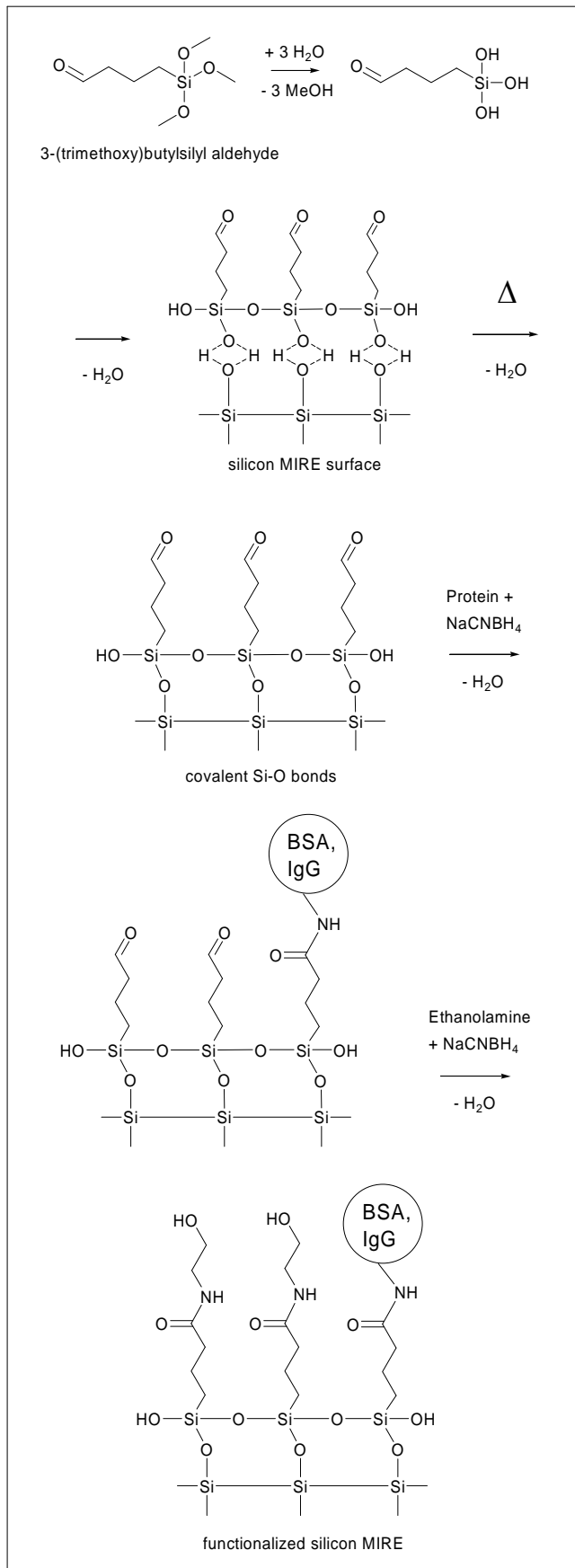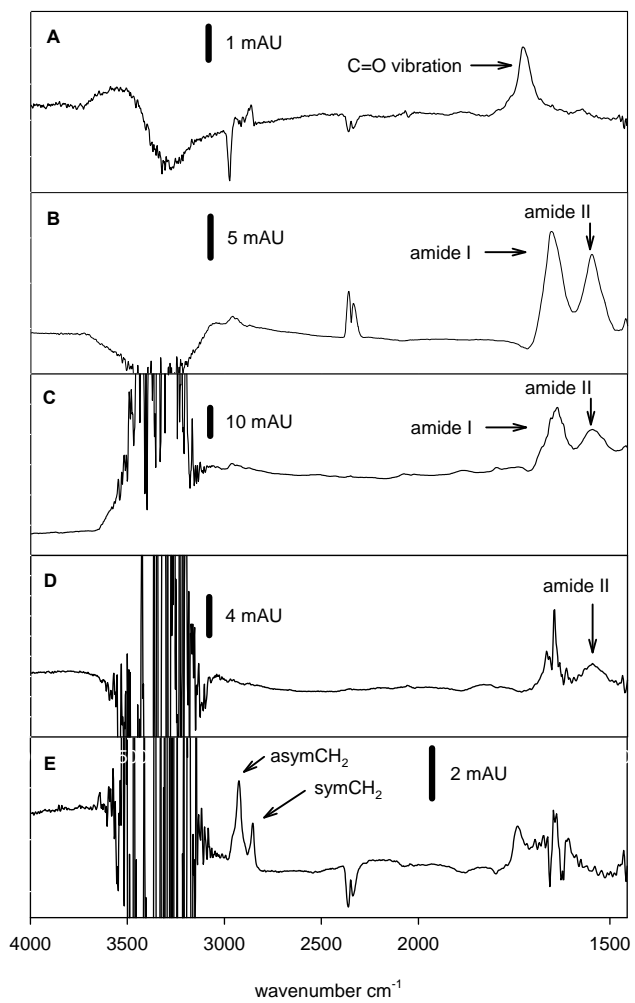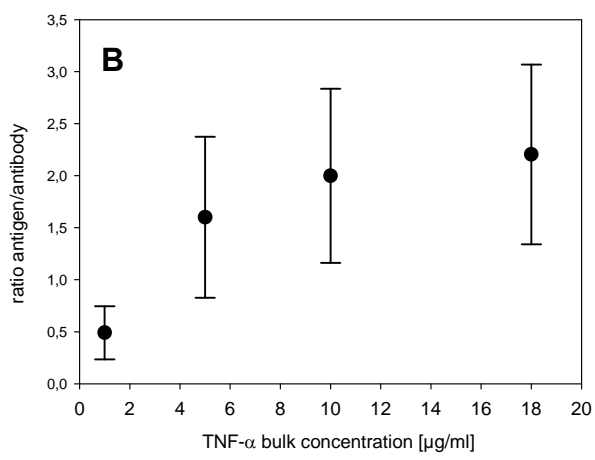
Fig. 1

3-(trimethoxy)butylsilyl aldehyde

silicon MIRE surface

covalent Si-O bonds
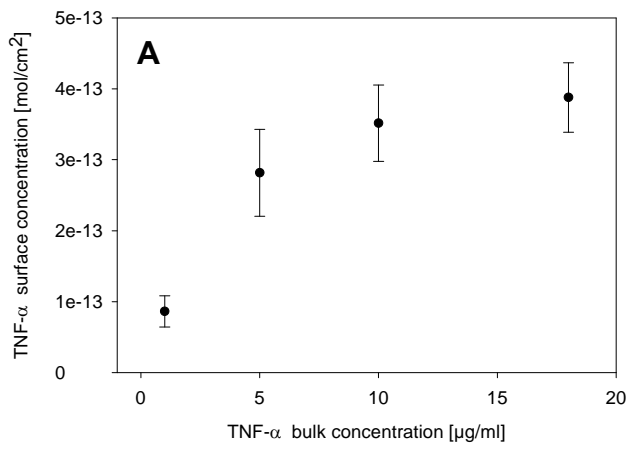
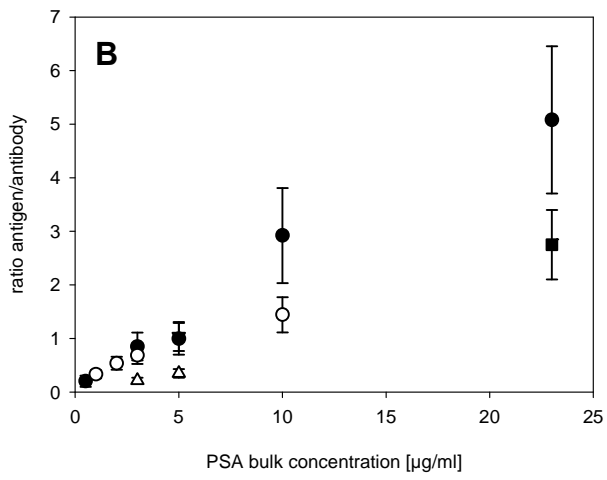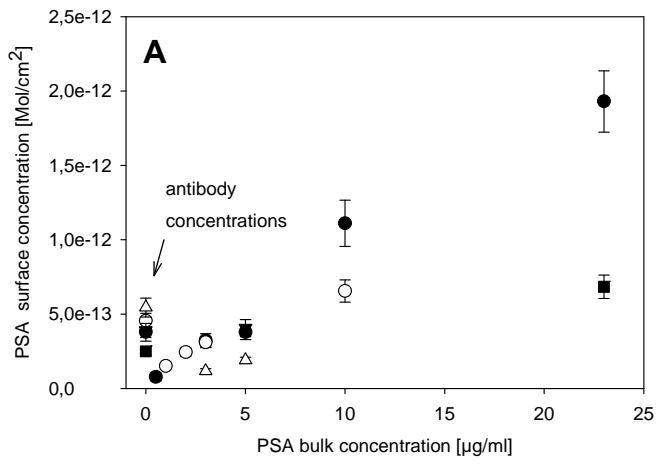functionalized silicon MIRE

Fig. 2

Fig. 3

Fig. 4

References

1. H. Hunt and A. Armani, *Nanoscale*, 2010, **2**, 1544–1559.
2. E. Stern, J. F. Klemic, D. A. Routenberg, P. N. Wyrembak, D. B. Turner-Evans, A. D. Hamilton, D. A. LaVan, T. M. Fahmy and M. A. Reed, *Nature*, 2007, **445**, 519-522.
3. N. Backmann, C. Zahnd, F. Huber, A. Bietsch, A. Plückthun, H.-P. Lang, H.-J. Güntherodt, M. Hegner and C. Gerber, *PNAS*, 2005, **102**, 14587–14592.
4. E. Stern, A. Vacic, N. K. Rajan, J. M. Criscione, J. Park, B. R. Ilic, D. J. Mooney, M. A. Reed and T. M. Fahmy, *Nature Nanotechnology*, 2010, **5**, 138-142.
5. E. Benesa, M. Gröschla, W. Burgera and M. Schmid, *Sensors and Actuators A: Physical*, 1995, **48**, 1-21.
6. L. Pang, J. Li, J. Jiang, G. Shen and R. Yu, *Analytical Biochemistry*, 2006, **358**, 99-103.
7. X. Wang, J. Zhou, J. Song, J. Liu, N. Xu and Z. L. Wang, *Nano Letters*, 2006, **6**, 2768-2772.
8. L. G. Carrascosa, M. Moreno, M. Alvarez and L. M. Lechuga, *Trends in Analytical Chemistry*, 2005, **25**, 196-206.
9. L. M. Lechuga, J. Tamayo, M. Álvarez, L. G. Carrascosa, A. Yufera, R. Doldán, E. Peralías, A. Rueda, J. A. Plaza, K. Zinoviev, C. Domínguez, A. Zaballos, M. Moreno, C. Martínez-A, D. Wenn, N. Harris, C. Bringer, V. Bardinal, T. Camps, C. Vergnenègre, C. Fontaine, V. Díaz and A. Bernad, *Sensors and Actuators B: Chemical*, 2006, **118**, 2-10.
10. P. Dutta, K. Hill, P. G. Datskos and M. J. Sepaniak, *Lab on a Chip*, 2007, **7**, 1184-1191.
11. J. H. Lee, K. S. Hwang, J. Park, K. H. Yoon, D. S. Yoon and T. S. Kim, *Biosensors and Bioelectronics*, 2005, **20**, 2157-2162.
12. J. I. Hahm and C. M. Lieber, *Nano Letters*, 2004, **4**, 41-54.
13. D. S. Kim, J. E. Park, J. K. Shin, P. K. Kim, G. Lim and S. Shoji, *Sensors and Actuators B: Chemical*, 2006, **117**, 488-494.
14. F. Patolsky, G. Zheng and C. M. Lieber, *Nat Protoc*, 2006, **1**, 1711-1724.
15. J. A. Ferguson, F. J. Steemers and D. R. Walt, *Anal. Chem.*, 2000, **72**, 5618-5624.
16. G. Zheng, F. Patolsky, Y. Cui, W. U. Wang and C. M. Lieber, *Nature Biotechnology*, 2005, **23**, 1294-1301.
17. C. Y. Hsiao, C. H. Lin, C. H. Hung, C. J. Su, Y. R. Lo, C. C. Lee, H. C. Lin, F. H. Ko, T. Y. Huang and Y. S. Yang, *Biosensors and Bioelectronics*, 2009, **24**, 1223-1229.
18. J. Kim, J. Cho, P. M. Seidler, N. E. Kurland and V. K. Yadavalli, *Langmuir*, 2010, **26**, 2599–2608.
19. G. Reiter, N. Hassler, V. Weber, D. Falkenhagen and U. P. Fringeli, *Biochimica et Biophysica Acta*, 2004, **1699**, 253– 261.
20. N. Hassler, D. Baurecht, G. Reiter and U. P. Fringeli, *J. Phys. Chem. C*, 2011, **115**, 1064–1072.
21. C. Nowak, M. G. Santonicola, D. Schach, J. Zhu, R. B. Gennis, S. Ferguson-Miller, D. Baurecht, D. Walz, W. Knoll and R. L. C. Naumann, *Soft Matter*, 2010, **6**, 5523-5532.
22. J. Matijasevic, N. Hassler, G. Reiter and U. P. Fringeli, *Langmuir*, 2008, **24**, 2588-2596.
23. D. Baurecht, G. Reiter, N. Hassler, M. Schwarzott and U. P. Fringeli, *Chimia*, 2005, **59**, 226-235.
24. J. M. Andanson and A. Baiker, *Chemical Society Reviews*, 2010, **39**, 4571-4584.
25. S. Reimann, A. Urakawa and A. Baiker, *Journal of Physical Chemistry C*, 2010, **114**, 17836-17844.
26. M. Mueller and B. Kessler, *Langmuir*, 2011, **just accepted**.
27. M. Mueller, W. Ouyang and B. Kessler, *Spectrochimica Acta, Part A: Molecular and Biomolecular Spectroscopy*, 2010, **77A**, 709-716.
28. A. M. Popa, S. Angeloni, T. Buergi, J. A. Hubbell, H. Heinzelmann and R. Pugin, *Langmuir*, 2010, **26**, 15356-15365.
29. B. Panella, A. Vargas, D. Ferri and A. Baiker, *Chem.Mater.*, 2009, **21**, 4316–4322.
30. D. M. Meier, A. Urakawa, R. Mäder and A. Baiker, *Rev. Sci. Instrum.*, 2008, **80**, 094101(094101-094111).
31. A. Vargas, I. Shnitko, A. Teleki, S. Weyeneth, S. E. Pratsinis and A. Baiker, *Applied Surface Science*, 2010, **257**, 2861-2869.
32. O. Taratula, E. Galoppini and R. Mendelsohn, *Langmuir*, 2009, **25**, 2107-2113.
33. R. Mendelsohn, G. Mao and C. R. Flach, *Biochimica et Biophysica Acta*, 2010, **1798**, 788-800.

34. U. P. Fringeli, in *Internal Reflection Spectroscopy*, ed. F. M. Mirabella Jr., CRC Press, New York, 1992, pp. 255-324.

35. U. P. Fringeli, D. Baurecht, T. Bürgi, M. Siam, G. Reiter, M. Schwarzott and P. Brüesch, in *Handbook of Thin Film Materials*, ed. H. S. Nalwa, Academic Press, San Diego (USA), 2002, vol. 2, pp. 191-229.

36. C. Heitzinger, Y. Liu, N. Mauser, C. Ringhofer and R. W. Dutton, *J. Comput. Theor. Nanosci.*, 2010, **7**, 2574–2580.

37. C. Heitzinger, N. Mauser and C. Ringhofer, *SIAM J. Appl. Math.*, 2010, **70**, 1634–1654.

38. S. Baumgartner and C. Heitzinger, *Commun. Math. Sci.*, 2012, **10**, 693–716.

39. A. Bulyha and C. Heitzinger, *Nanoscale*, 2011, **3**, 1608-1617.

40. L. De Vico, L. Iversen, M. H. Sørensen, M. Brandbyge, J. Nygård, K. L. Martinez and J. H. Jensen, *Nanoscale*, 2011, **3**, 3635–3640.

41. L. De Vico, M. H. Sørensen, L. Iversen, D. M. Rogers, B. S. Sørensen, M. Brandbyge, J. Nygård, K. L. Martinez and J. H. Jensen, *Nanoscale, 2011, 3, 706-717*, 2011, **3**, 706-717.

42. S. Baumgartner, M. Vasicek and C. Heitzinger, Analysis of field-effect biosensors using self-consistent 3D drift-diffusion and Monte-Carlo simulations, Proc. Eurosensors XXV, Athens, September 2011.

43. S. Baumgartner, M. Vasicek, A. Bulyha and C. Heitzinger, *Nanotechnology*, 2011, **22(425503)**, 1-8.

44. S. Baumgartner, M. Vasicek and C. Heitzinger, *Procedia Engineering*, At press.

45. H. Guenzler and H. U. Gremlich, *IR-Spektroskopie*, Wiley-VCH, Weinheim, 2000.

46. N. J. Harrick, *Internal Reflection Spectroscopy*, Harrick Sci. Corp., Ossining (New York), 1979.

47. J. Matijasevic, Ph.D. Thesis, University of Vienna, 2008.

48. J. Zhang, J. Hoogboom, P. H. J. Kouwer, A. E. Rowan and T. Rasing, *J. Phys. Chem. C*, 2008, **112**, 20105–20108.

49. T. Maruyama, S. Katoh, M. Nakajima, H. Nabetani, T. P. Abbott, A. Shono and K. Satoh, *Journal of Membrane Science*, 2001, **192**.

50. K. Murayama and M. Tomida, *Biochemistry*, 2004, **42**, 11526-11532.

51. Y. S. Wei, S. Y. Lin, S. L. Wang, M. J. Li and W. T. Cheng, *Biopolymers (Biospectroscopy)*, 2003, **72**, 345–351.

52. O. Mori and T. Imae, *Colloids and Surfaces B: Biointerfaces*, 1997, **9**, 31-36.

53. M. Tencera, R. Charbonneaua, N. Lahouda and P. Berini, *Applied surface science*, 2007, **253**, 9209-9214.

54. N. Hassler, Ph.D. Thesis, University of Vienna, 2008.

55. Y. S. Lin and V. Hlady, *Colloids and Surfaces B: Biointerfaces*, 1994, **2**, 481-491.

56. G. Scatchard and W. T. Yap, *J. Am. Chem. Soc.*, 1964, **86**, 3434.

57. J. K. Luey, J. McGuire and R. D. Sproull, *Journal of Colloid and Interface Science*, 1991, **143**, 489-500.

58. R. L. Brady, R. E. Hubbard, D. J. King, D. C. Low, R. S.M. and R. J. Todd, *J.Mol.Biol.*, 1991, **219**, 603.

59. C. J. Roberts, P. M. Williams, J. Davies, A. C. Dawkes, J. Sefton, J. C. Edwards, A. G. Haymes, C. Bestwick, M. C. Davies and S. J. B. Tendler, *Langmuir*, 1995, **11**, 1822-1826.